Engineering Structures 153 (2017) 136–145

Contents lists available at ScienceDirect

Engineering Structures

journal homepage: www.elsevier.com/locate/engstruct

An experimentally validated finite element formulation for modeling 3D rotational energy harvesters

J.M. Ramírez[a,*], C.D. Gatti[a], S.P. Machado[a], M. Febbo[b]

[a] Consejo Nacional de Investigaciones Científicas y Técnicas (CONICET), Grupo de Investigación en Multifísica Aplicada (GIMAP), Universidad Tecnológica Nacional FRBB (UTN), 11 de Abril 461, 8000 Bahía Blanca, Argentina

[b] Instituto de Física del Sur (IFISUR), Consejo Nacional de Investigaciones Científicas y Técnicas (CONICET) and Departamento de Física, Universidad Nacional del Sur (UNS), Av. Alem 1253, 8000 Bahía Blanca, Argentina

ARTICLE INFO

Keywords:
Finite element method
Rotating beam
Piezoelectric material
Energy harvesting
Arduino board
Wireless sensor
Bluetooth

ABSTRACT

Piezoelectric energy harvesting devices convert mechanical energy into electrical energy due to the mechanical deformations of the structures. Energy harvesting prototypes are used to feed low-power electronic devices and sensors. In this work, a one-dimensional finite element is developed for modeling three-dimensional rotational energy harvesters. The rotating piezoelectric beam is formulated by means of a geometrically nonlinear finite element with six mechanical degrees of freedom and one electrical degree of freedom per node. Using Timoshenko beam theory for the mechanical domain and a first-order theory for the electrical field, the electromechanical equilibrium equations of motion are then derived using D'Alembert principle. In order to validate our finite element formulation, two energy harvesting devices are built and tested, getting insights into the generation of electrical power, natural frequencies and time responses of the dynamical variables. An Arduino board is implemented as the data acquisition system that transfers the voltage signal via Bluetooth, avoiding the complexity of slip-rings mechanisms for data transmission. Finally, the results of our formulation are compared with those obtained using a commercial software (Abaqus) and the experimental results. A good correlation between the three methods is obtained, providing evidence that our formulation accurately predicts the behavior of rotational energy harvesters.

1. Introduction

The dynamic behavior of rotating structures has been studied for many years. There are numerous reports in the literature that analyze the vibration of rotating beams. Carnegie [1] investigated the vibration of rotating cantilever blading, obtaining a theoretical expression for the work done due to centrifugal and Coriolis effects. Boyce and Handelman [2] studied the transverse vibration and the influence of a tip mass placed at the free end of a cantilever beam taking into account a constant speed. Hoa [3] proposed a finite element (FE) method to investigate the vibration frequency of a rotating cantilever beam with a tip mass. The finite element method was based on a third-order polynomial for the variation of the lateral displacement. Geradin and Kill [4] developed a new approach to finite element modeling applied to flexible rotors in order to perform the stability analysis. Their models were developed with the rotating frame and the inertial frame approaches. In both cases an asymmetric finite element is proposed. Aircraft wings and blades are applications of the investigations about the dynamic behavior of rotating structures. Recently, composite materials have been widely used in the main structure for increasing the performance of the blades or wings. Saravia et al. [5] investigated the dynamic stability behavior of thin-walled rotating composite beams using the finite element method. Due to the flexibility of composite structures, control of the vibrations is essential [6]. For this reason, in the last decades the inclusion of smart materials in the main structure has been studied. The suppression of vibrations is improved using active control in the structures with piezoelectric actuators. Piezoelectric materials are usually of interest when designing smart structures that can be used as sensors or actuators [7,8]. In the last few years, energy harvesting has received increasing attention due to its applications. It converts the waste energy into usable electrical energy, or in other words, mechanical vibrations are converted into electrical energy used to power mobile devices and wireless sensors networks [9]. Many researchers have derived mathematical models for energy harvesting beams [10]; most of them have used the Euler–Bernoulli beam theory with a harmonic base excitation. Erturk and Inman [11,12] studied a distributed parameter electromechanical model for cantilevered piezoelectric energy harvesters. Mitcheson et al. [13] presented a state-of-

* Corresponding author.
E-mail address: josemramire@gmail.com (J.M. Ramírez).

http://dx.doi.org/10.1016/j.engstruct.2017.10.027
Received 8 May 2017; Received in revised form 9 October 2017; Accepted 10 October 2017

art review of energy harvesting devices including possible applications and future developments.

Finite element plate models are also used to investigate piezoelectric structures under base harmonic motion. Marqui Junior et al. [14] proposed an electromechanical coupled finite element plate model for predicting the electrical power output of piezoelectric energy harvester plates. The excitation is due to the harmonic motion of the base in the transverse direction. Detwiler et al. [15] formulated a laminated composite plate with piezoelectric material to analyze the mechanical-electrical behavior. The top and bottom surface of the beam were subjected to an electric potential of 1 V across the thickness of the beam, and the corresponding displacements were determined. On the other hand, there are several finite element software packages (such as Abaqus or ANSYS) for the modeling of piezoelectric materials. Kumar et al. [16] analyzed the performance of lead-free piezoelectric materials in unimorph cantilever piezoelectric energy harvesters. The finite element method was used to model the piezoelectric structure, while genetic algorithm optimization was used to optimize the power output. Staworko and Uhl [17] presented an overview of modeling techniques of piezoelectric elements and their comparison with commercial software for simulating electromechanical systems. The models built using Simulink and PSPICE give a slight difference of the frequency of vibration with respect to Ansys simulation, whereas the amplitudes of the time response using Simulink and PSPICE are three times larger than those obtained with Ansys. Elvin et al. [18] developed a coupled finite element-circuit simulation model using finite element software packages. For the mechanical domain, a finite element method was used to calculate the dynamic response. In the electronic domain, the simulation tool SPICE was used to calculate the electrical response. This approach allows for the modeling of complex mechanical geometries. However, the solution technique is computationally expensive for large models. Zhou et al. [19] proposed an equivalent SDOF system to describe the energy harvesting performance of a cantilever beam. The peak output power and voltage were compared with numerical simulation using the commercial FE package Ansys.

In the last few years a number of investigations have been published about rotational energy harvesters. Gu and Livernore [20] presented a single-degree-of-freedom (SDOF) model taking into account the centrifugal force of the tip mass of a passive self-tuning energy harvester for rotational vibration applications. Khameneifar et al. [21,22] also presented an analytical model with a SDOF considering the centrifugal force of the tip mass and the gravity force of the whole model. Guan and Liao [23] developed a novel design of a rotating harvesting structure using an analytical model that assumes the whole system mass in the centrifugal and gravity forces. They analyzed the device theoretically and experimentally. Their results do not predict with sufficient accuracy the experimental results. Shahruz and Sundararajan [24] proposed a SDOF mathematical model of a cantilever beam with a tip mass considering the whole system mass in centrifugal and gravity forces. They provided a guideline for the scavenger parameters in order to have it resonate. Yang et al. [25] investigated experimentally an improved the output power of a rotational piezoelectric wind energy harvester. They proposed an impact force to enable effective excitation. On the other hand, Hsu et al. [26] used a finite element software package (COMSOL) to simulate a rotating cantilever beam with a tip mass. They analyzed self-frequency tuning piezoelectric energy harvesters for rotational motion. Their FE model takes into account the shear deformation, piezoelectric effect, and stress stiffening effect induced by the centrifugal forces of the entire mass. Their results were compared with an analytical model and experimental tests.

In the above references the analysis of energy harvesting devices was limited to simple geometries such as cantilever beams [20–22]. In Refs. [23,24] the centrifugal and gravitational forces applied to the SDOF system were considered in the FE model, but the softening effect induced by the rotation speed was neglected. In [26] Hsu et al. developed a FE model using a commercial software (COMSOL) based on three dimensional (3D) solid elements to model the rotational energy harvester. This approach allows to solve the difficulties mentioned above, but it has a large computational cost due to the 3D elements. In the present work, in contrast to current scientific literature, a one-dimensional finite element is developed to model 3D rotational energy harvesting devices. Within this approach it is possible to model complex geometric configurations, the geometrically nonlinear effect induced by the centrifugal forces and the electromechanical coupling. The piezoelectric beam is formulated by linearizing a geometrically nonlinear FE with six mechanical degrees of freedom per node and one electrical degree of freedom interpolated using standard linear shape functions. Timoshenko beam theory is used for the mechanical domain [5], and a first order theory is used for the electrical domain [31].

The present article is organized as follows. After the introduction, the kinematics of a piezoelectric rotating beam is presented in Section 2. Section 3 presents the details of the variational principle to derive the equilibrium equations of motion of the problem using D'Alembert principle. Section 4 presents the formulation of the piezoelectric beam element. Section 5 contains the experimental setup to validate our FE approach. Section 6 shows a comparison of the natural frequencies between our FE formulation and the numerical simulations using Abaqus. The voltage time response and the voltage and power generation of our proposed model are also compared with the experimental results. Finally, Section 7 presents the conclusions.

2. Kinematics

The main aspects of the present rotational energy harvester formulation are the following:

- The kinematics is based on the Timoshenko theory.
- The electrical potential is a linear interpolation through the thickness.
- The piezoelectric material obeys a linear constitutive equation.

2.1. Reference system

The global and local Cartesian reference systems are mainly used as shown in Fig.1.

- Global reference system {O, x, y, z}.
- Local reference system {T, X′, Y′, Z′}.

A 3D beam is a solid of length L oriented in the longitudinal direction X'. The transverse area A with dimensions in $Y'Z'$ plane is orthogonal to X' and it is relatively small with respect to the longitudinal direction. Point c is the shear center of the beam. If the shear center c and the neutral point T do not coincide, a coupling between axial/bending and bending in x and y direction exists. The points T, g (neutral point, gravity center) and c coincide for homogenous solid sections.

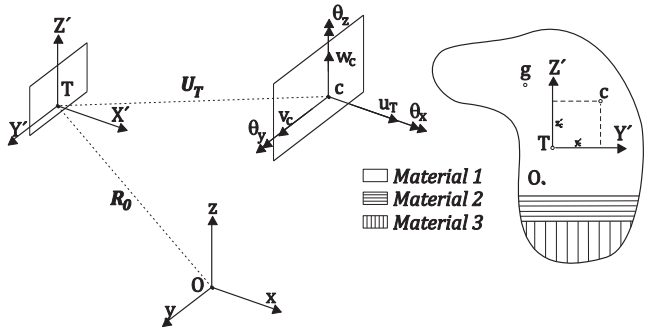

Fig. 1. Global reference systems: {O, x, y, z} and local reference systems {T, X′, Y′, Z′}. Gravity and shear centers (g and c).

Instead they do not coincide for composite beams.

2.2. Displacements

The Timoshenko beam theory is used for obtaining the dynamics of a rotating beam [27]. This beam theory is appropriate in order to include the linearization of the formulation by means of a geometrically non-linear finite element. It assumes that the shear center c and T do not coincide, and hence a coupling between axial, bending/shear and torsion effects exists. Working with the global system {O, x, y, z}, the following displacement field for an arbitrary point of coordinates (x, y, z) can be obtained:

$$\begin{bmatrix} u \\ v \\ w \end{bmatrix} = \begin{bmatrix} u_T(x,t) + z\theta_y(x,t) - y\theta_z(x,t) \\ v_c(x,t) - (z - z_c)\theta_x \\ w_c(x,t) + (y - y_c)\theta_x \end{bmatrix} \tag{1}$$

$$\boldsymbol{U} = [u(x,t), v(x,t), w(x,t), \theta_x(x,t), \theta_y(x,t), \theta_z(x,t)]^T \tag{2}$$

where u, v and w are the global displacements, y_T and z_T are the coordinates of T, and y_c and z_c are the coordinates of c. In the local system {T, X′, Y′, Z′}, the displacement can be rewritten as:

$$\boldsymbol{U_T} = [u_t(x',t), v_c(x',t), w_c(x',t), \theta_x(x',t), \theta_y(x',t), \theta_z(x',t)]^T \tag{3}$$

where the apostrophe indicates that the quantity is related to such local system. This system is parallel to the global system; displacements have the same values in both systems, which implies that no apostrophe is needed.

The instantaneous position vector of a point in the deformed configuration [28] can be written as:

$$\boldsymbol{R} = \boldsymbol{R}_0 + \boldsymbol{S_M}\boldsymbol{U} \tag{4}$$

where $\boldsymbol{R}_0$ is the point of the beam in the non-deformed configuration (hub length), and $\boldsymbol{S_M}$ is the cross sectional matrix.

2.3. Velocity and acceleration vectors

For the general case of a structural element that is rotating in space, we can write the absolute velocity and acceleration of a point of the beam [5]. The generalized velocities and accelerations are defined as:

$$\mathbf{V_G} = [\dot{u}(x,t), \dot{v}(x,t), \dot{w}(x,t), \dot{\theta}_x(x,t), \dot{\theta}_y(x,t), \dot{\theta}_z(x,t)]^T \tag{5}$$

$$\boldsymbol{a_G} = [\ddot{u}(x,t), \ddot{v}(x,t), \ddot{w}(x,t), \ddot{\theta}_x(x,t), \ddot{\theta}_y(x,t), \ddot{\theta}_z(x,t)]^T \tag{6}$$

2.4. Strain field

Let us consider the Green-Lagrange strain tensor according to [29]:

$$L_{ij} = \frac{1}{2}(u_{i,j} + u_{j,i} + u_{k,i}u_{k,j}) \tag{7}$$

where

$$u_{i,j} = \frac{\partial u_i}{\partial X_j} \tag{8}$$

The Green-Lagrange strain in vector form is expressed as:

$$\boldsymbol{\varepsilon_R} = \boldsymbol{S_T}\,\boldsymbol{\varepsilon_G} \tag{9}$$

where $\boldsymbol{\varepsilon_G}$ is the generalized strain, and $\boldsymbol{S_T}$ is the strain transformation matrix. The three non-zero components of the Green strain are $\boldsymbol{\varepsilon_{xx}}$, $\boldsymbol{\varepsilon_{xy}}$, $\boldsymbol{\varepsilon_{xz}}$. Eq. (9) takes into account only the nonlinear components of the simplified Green Lagrange strains corresponding to the axial-bending coupling.

2.5. Constitutive equations

The components of the stress and the electric displacement tensor can be derived from the electric enthalpy density as [30]:

$$\sigma_{ij} = \frac{\partial H}{\partial_{ij}},\ D_i = -\frac{\partial H}{\partial E_i} \tag{10}$$

The form of the electric enthalpy density in the linearized theory of piezoelectricity is:

$$H = \frac{1}{2}C_{ijkl}\varepsilon_{ij}\varepsilon_{kl} - e_{kij}E_k\varepsilon_{ij} - \frac{1}{2}\varepsilon_{ij}^S E_i E_j \tag{11}$$

where C_{ijkl} are the elastic constants, e_{kij} are the piezoelectric constants, and ε_{ij}^S are the permittivity constants. The superscript s denotes that the respective constants are evaluated at constant strain.

Using Eqs. (10) and (11) along with the relation $\partial\varepsilon_{ij}/\partial\varepsilon_{ji} = \delta\varepsilon_{ij}$, where δ_{ij} is the Kronecker delta, we obtain the linear constitutive equations, given as:

$$\begin{bmatrix} \boldsymbol{\sigma} \\ \boldsymbol{D} \end{bmatrix} = \begin{bmatrix} \widetilde{\boldsymbol{C}} & \widetilde{\boldsymbol{e}}^T \\ \widetilde{\boldsymbol{e}} & \boldsymbol{\varepsilon} \end{bmatrix} \begin{bmatrix} \boldsymbol{\varepsilon_G} \\ \boldsymbol{E} \end{bmatrix} \tag{12}$$

where $\widetilde{\boldsymbol{C}}$, $\widetilde{\boldsymbol{e}}$ and $\widetilde{\boldsymbol{\varepsilon}}$ are the elasticity tensor, the piezoelectric tensor and the permittivity tensor, respectively. It must be noted that $\boldsymbol{\varepsilon_G}$ and $\boldsymbol{\sigma}$ are the generalized strain and stress matrices, respectively. $\boldsymbol{E}$ and $\boldsymbol{D}$ are the electric field and electric displacement vectors.

2.6. Electric field vector

The definition of the electric field vector in terms of electric potential is:

$$\boldsymbol{E} = -\nabla\phi \tag{13}$$

Now the electric field is defined as [31]:

$$\overline{\boldsymbol{E}} = -\overline{\boldsymbol{A}}\,\overline{\boldsymbol{\phi}} \tag{14}$$

where $\overline{\phi}$ is the electric degree of freedom.

$$\overline{\phi} = [\phi_x \ \ \phi_{y,y} \ \ \phi_{z,z} \ \ \phi_{x,x} \ \ \phi_{y,yx} \ \ \phi_{z,zx}]^T \tag{15}$$

The function for the electrical potential [32] is:

$$\phi(x,y,z) = \phi_x(x) + y\frac{\partial}{\partial y}\phi_y(x) + z\frac{\partial}{\partial z}\phi_z(x) \tag{16}$$

$\overline{\boldsymbol{A}}$ is the electrical transformation:

$$\overline{\boldsymbol{A}} = \begin{bmatrix} 0 & 0 & 0 & 1 & y' & z' \\ 0 & 1 & 0 & 0 & 0 & 0 \\ 0 & 0 & 1 & 0 & 0 & 0 \end{bmatrix} \tag{17}$$

The electrical potential is constant in this case.

$$\frac{\partial}{\partial z}\phi_z(x) = E_3 = -\frac{\mathrm{v}}{h_e} \tag{18}$$

The electrical constitutive matrix $\overline{\overline{D}}$ is obtained by integration over the cross section:

$$\overline{\overline{D}} = \int_A \overline{\boldsymbol{A}}^T \boldsymbol{D}\ d\boldsymbol{A} \tag{19}$$

This expression is similarly obtained by the stress resultant of the beam [32].

3. Variational formulation

To derive the equilibrium equations of the problem, the d'Alembert principle is used [33]. The principle of virtual work for dynamical systems is:

$$\delta\Pi = \delta W_{int} - \delta W_E + \delta W_T \tag{20}$$

3.1. Virtual strain energy

Let us compute the strain energy as a contribution from the elastic

and electric energy:

$$\delta W_{int} = \delta W_{int}^{d} + \delta W_{int}^{e} = \int_{V}^{\delta} (\boldsymbol{\sigma}\boldsymbol{\varepsilon}_R) dA + \int_{V}^{\delta} (\overline{\boldsymbol{E}}^T \overline{\boldsymbol{D}}) dV \tag{21}$$

The first integral is due to the elastic deformation of the body [34], and the second integral comes from the electrostatic energy which is equal to the work done by the moving charge while it moves from a cathode to an anode. The electric field is constant between electrodes:

$$\overline{\boldsymbol{E}} = \begin{bmatrix} 0 & 0 & -\dfrac{\mathrm{v}}{h_e} \end{bmatrix}^T \tag{22}$$

where h_e is the electrode distance.

3.2. Virtual work of d'Alembert forces

The virtual work of the inertia forces is defined as:

$$\delta W_T = \int_V \rho \ddot{\boldsymbol{R}}^T \delta \boldsymbol{R} dV \tag{23}$$

The inertia forces provide for two terms, the relative and centrifugal inertia [4].

3.3. Virtual work of the external forces

The virtual work of the external forces can be expressed as:

$$\delta W_E = \delta \boldsymbol{U} \boldsymbol{F_E} \tag{24}$$

where $\boldsymbol{F_E}$ is a vector that represents the external forces.Additionally, the virtual work of the non-conservative force for the electrical charge is:

$$\delta Q_E = \delta \boldsymbol{V} \boldsymbol{Q_E} \tag{25}$$

where $\boldsymbol{Q_E}$ is a vector that represents the electrical load.

4. Finite element formulation

The finite element method provides an approach for the discretization of a continuum [35]. In this analysis, the beam has 2 nodes per element with 12 mechanical degrees of freedom per element, 6 at each node (3 displacements and 3 rotations) and 2 electrical degrees of freedom per element. Introducing the finite element discretization, the generalized strains in the generalized nodal displacements are:

$$\boldsymbol{U} = \boldsymbol{N}(\eta)\widehat{\boldsymbol{U}} \tag{26}$$

$$\boldsymbol{N}(\eta) = \sum_{i=1}^{n} \boldsymbol{N}_i(\eta) \boldsymbol{I}_6 \tag{27}$$

In the above equations, $\boldsymbol{N}$ is the linear shape function matrix, $\widehat{\boldsymbol{U}}$ is the nodal displacement, $\widehat{\boldsymbol{X}}$ is the nodal coordinate, and $\boldsymbol{I}_6$ is the 6 × 6 unit matrix. The generalized strain matrix is:

$$\boldsymbol{\varepsilon_R} = \boldsymbol{B}_i \widehat{\boldsymbol{U}} \tag{28}$$

where $\boldsymbol{B}_i$ is the displacement-deformation matrix according to the strain tensor of node i. The electric field vector is defined as:

$$\overline{\boldsymbol{E}} = -\boldsymbol{B_E}\widehat{\boldsymbol{V}} \tag{29}$$

where $\widehat{\boldsymbol{V}}$ is the nodal voltage, and $\boldsymbol{B_E}$ is:

$$\boldsymbol{B_E} = [0 \quad 0 \quad 1/h_e]^T \tag{30}$$

It is important to mention that a linear interpolation through the thickness for the electric potential is used because the electric field of the piezoelectric material MIDE QP16N is constant in the thickness.

4.1. Tangent stiffness

Introducing Eq. (9) into the virtual strain energy expression Eq. (21), we obtain:

$$\delta W_{int} = \delta W_{int}^{d} + \delta W_{int}^{e} \tag{31}$$

$$\delta W_{int}^{d} = \int_{L}^{\delta} (\boldsymbol{B}\widehat{\boldsymbol{U}})^T \boldsymbol{C}\boldsymbol{B}\widehat{\boldsymbol{U}} dx + \int_{L} \overline{\boldsymbol{E}}^T \boldsymbol{e}^T \delta(\boldsymbol{B}\widehat{\boldsymbol{U}}) \boldsymbol{dx} \tag{32}$$

$$\delta W_{int}^{e} = \int_{L}^{\delta} (\boldsymbol{B_E}\widehat{\boldsymbol{V}})^T \boldsymbol{e}^T \boldsymbol{B}\widehat{\boldsymbol{U}} dx - \int_{L}^{\delta} (\boldsymbol{B_E}\widehat{\boldsymbol{V}})^T \boldsymbol{\varepsilon}^s \boldsymbol{B_E}\widehat{\boldsymbol{V}} dx \tag{33}$$

Eqs. (32) and (33) can be rewritten as:

$$\delta W_{int}^{d} = \delta \widehat{\boldsymbol{U}}^T \boldsymbol{K_M} \widehat{\boldsymbol{U}} + \delta \widehat{\boldsymbol{U}}^T \boldsymbol{K_G} \widehat{\boldsymbol{U}} - \delta \widehat{\boldsymbol{U}}^T \boldsymbol{\Theta} \widehat{\boldsymbol{V}} \tag{34}$$

$$\delta W_{int}^{e} = \delta \widehat{\boldsymbol{V}}^T \boldsymbol{\Theta}^T \widehat{\boldsymbol{U}} - \delta \widehat{\boldsymbol{V}}^T \boldsymbol{C_P} \widehat{\boldsymbol{V}} \tag{35}$$

where $\boldsymbol{K_M}$, $\boldsymbol{K_G}$, $\boldsymbol{\Theta}$, $\boldsymbol{C_P}$ are the material and geometric stiffness, and the electromechanical and capacitance matrices, respectively. Note that the electric field is assumed to be uniform for d_{31} harvesting mode, and the coupling matrix is given by:

$$\boldsymbol{\Theta} = \int_{L}^{\delta} (\boldsymbol{B_E}\widehat{\boldsymbol{V}})^T \boldsymbol{e}^T \boldsymbol{B}\widehat{\boldsymbol{U}} dx \tag{36}$$

Now, in order to consider the non-uniform electric field for d_{33} harvesting mode, we assume the empirical approach [36], yielding the following coupling matrix:

$$\boldsymbol{\Theta} = \alpha \int_{L}^{\delta} (\boldsymbol{B_E}\widehat{\boldsymbol{V}})^T \boldsymbol{e}^T \boldsymbol{B}\widehat{\boldsymbol{U}} dx \tag{37}$$

where α is an empirical constant that is used to consider the non-uniform electric field.

4.2. Geometric stiffness matrix

The geometric stiffness matrix can be expressed as:

$$\boldsymbol{K_G} = T(x)\boldsymbol{K_G^U} \tag{38}$$

where $T(x)$ is the axial beam force acting on any section at a distance x from the inner edge of the element [5], and $\boldsymbol{K_G^U}$ is a unit geometric stiffness matrix.

4.3. Dynamic matrices

Introducing the finite element approximations in Eqs. (5) and (6):

$$\boldsymbol{R}_0 = \boldsymbol{H}\widehat{\boldsymbol{X}},\ \boldsymbol{V_G} = \boldsymbol{N}\widehat{\boldsymbol{V}}_G,\ \boldsymbol{a_G} = \boldsymbol{N}\hat{\boldsymbol{a}}_G,\ \boldsymbol{U} = \boldsymbol{H}\widehat{\boldsymbol{U}} \tag{39}$$

where $\boldsymbol{N}$ is the inertia shape function, $\widehat{\boldsymbol{X}}$ is the nodal coordinate, $\widehat{\boldsymbol{U}}$ is the nodal displacement, $\widehat{\boldsymbol{V}}_G$ is the nodal velocity, and $\hat{\boldsymbol{a}}_G$ is the nodal acceleration.Introducing Eq. (39) into Eq. (23) yields:

$$\delta W_T = (\hat{\boldsymbol{a}}_G^T \boldsymbol{M} + \boldsymbol{K_R}\widehat{\boldsymbol{U}} + \boldsymbol{C_c}\widehat{\boldsymbol{V}}_G)\delta\widehat{\boldsymbol{U}} \tag{40}$$

where $\boldsymbol{M}$, $\boldsymbol{K_R}$, $\boldsymbol{C_C}$ are the mass matrix, the rotation stiffness matrix and the coriolis matrix, respectively. Note that the rotation stiffness plays the role of a negative stiffness.

4.4. Equation of motions

The electromechanical equation of motion is formulated in matrix form as:

$$\boldsymbol{K_T}\widehat{\boldsymbol{U}} + \boldsymbol{D}\widehat{\boldsymbol{V}}_G + \boldsymbol{C_c}\widehat{\boldsymbol{V}}_G + \boldsymbol{M}\hat{\boldsymbol{a}}_G - \boldsymbol{\Theta}\widehat{\boldsymbol{V}} = \boldsymbol{F_E} \tag{41}$$

$$\boldsymbol{\Theta}^T\widehat{\boldsymbol{U}} + \boldsymbol{C_P}\widehat{\boldsymbol{V}} + \boldsymbol{Q_E} = 0 \tag{42}$$

where the total stiffness matrix and the damping matrix are, respectively:

$$\boldsymbol{K_T} = \boldsymbol{K_M} + \boldsymbol{K_G} + \boldsymbol{K_R} \tag{43}$$

$$\boldsymbol{D} = \alpha\boldsymbol{M} + \beta\boldsymbol{K_T} \tag{44}$$

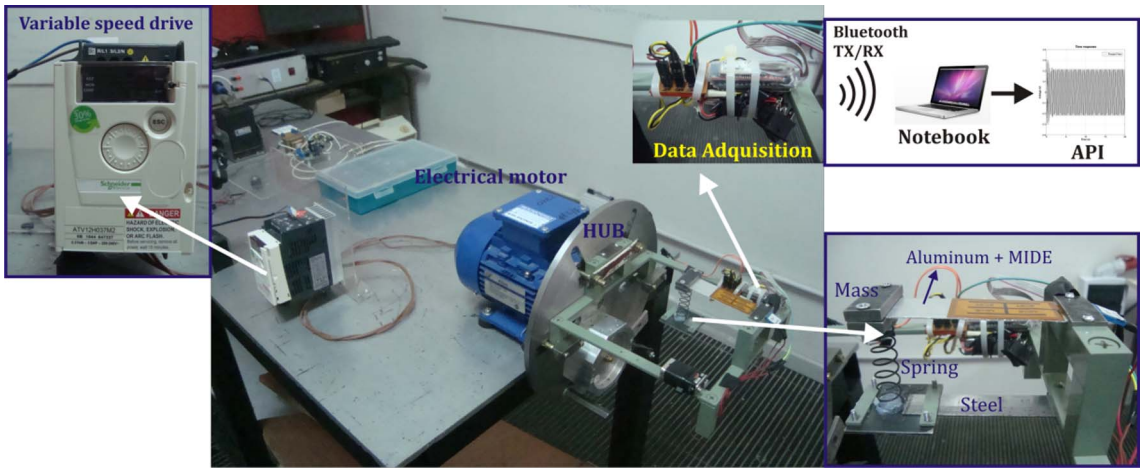

Fig. 2. Experimental setup to test the rotational energy harvester.

5. Experimental setup

5.1. Testing system description

The experimental setup built to assess the dynamic behavior of the rotational energy harvester is shown in Fig. 2.

The harvesting system is placed on a rigid frame that rotates at a constant angular velocity with respect to its axis of rotation, which is parallel to the longitudinal axis. The harvester device is mounted on the hub at 55 mm from the axis of rotation, which is excited by a constant rotation speed. A variable speed drive is used to control the speed of a 3-Phase Electric Motor of 0.37 KW (manufactured by Altium). An Arduino board is used to read out the voltage signal in real-time, and the selected communication protocol was Bluetooth (at 115,200 baud) because it is available in almost every mobile device, and also in computers. The proposed acquisition system has two main parts: hardware and software. The hardware consists of the Arduino platform, a Bluetooth receiver-transmitter and a notebook. In the case of acquisition, the mechanical motion is converted through the piezoelectric material into electrical energy. Those signals are acquired through the analog input ports on the Arduino board, and then converted using the internal analog-to-digital converter. It is important to note that the Arduino board is energized by a 9 V battery due to the fact that this is the first design of the energy harvester; in future works, our goal is to remove the battery and convert the system into a proper (self-energized) energy harvesting device. As for the software, an application programming interface (API) is developed to establish a starting/stopping routine with the Bluetooth connection to save the acquired data (100 samples per seconds). Note that in the experimental tests reported in [20–26] data was acquired using wires connected to a slip ring.

5.2. Experimental test configuration

In this work, two devices are tested to validate our FE formulation with the aim of getting insight into the electrical power generation, natural frequencies and voltage time responses. First, a cantilever beam with a mass at the free end is tested to verify its performance reliability at different rotation speeds, as shown in Fig. 3. The cantilever structure is mounted on the hub at 55 mm from the axis of rotation in the X direction. The substrate is made of aluminum, and its dimensions are 25 mm × 0.5 mm × 79 mm. The MIDE piezoelectric sheet bonded to the substrate has dimensions of 20.57 mm × 0.254 mm × 45.8 mm. The tip mass is made of steel, with dimensions of 28 mm × 4 mm × 16 mm. The piezoelectric performance is analyzed at low frequencies of rotation from 1 Hz to 5 Hz.

The second device is made of two beams with masses at the free ends linked with a spring as shown in Fig. 4. The top beam structure is made of aluminum, with dimensions of 25 mm × 0.5 mm × 79 mm; its tip mass is made of steel, whose dimensions are 38 mm × 10 mm × 16 mm. The bottom beam structure is made of steel, and with dimensions are 19 mm × 1 mm × 63 mm; its tip mass is made of steel, with dimensions 45 mm × 2 mm × 45 mm. The piezoelectric performance is analyzed at frequencies of rotation from 1 Hz to

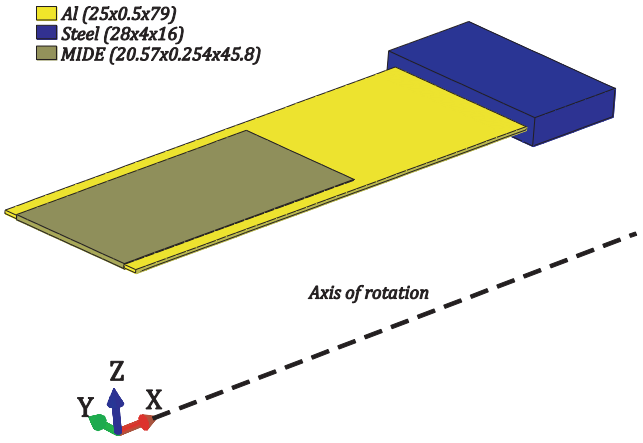

Fig. 3. Cantilever piezoelectric rotating beam with a tip mass at the free end.

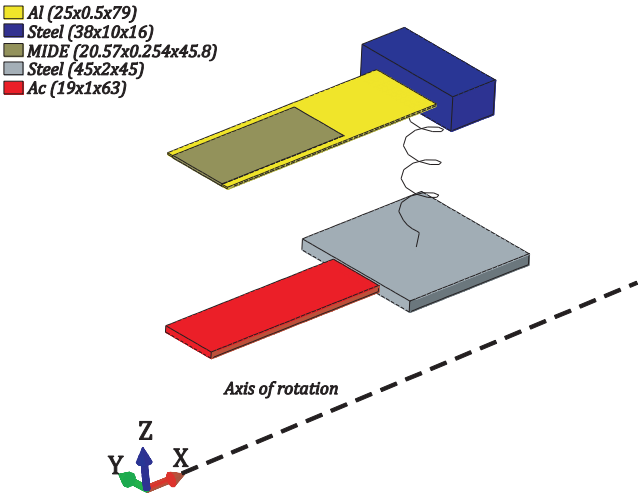

Fig. 4. Two piezoelectric rotating beams with a tip mass and a spring linked at the free end.

Table 1
Material properties for aluminum, steel, spring and MIDE QP16N.

Aluminum		MIDE QP16N		Spring		Steel	
Young's modulus	67 GPa	Young's modulus	67 GPa	Stiffness	560 N/m	Young's modulus	210 GPa
Density	2700 kg/m^3	Density	7800 kg/m^3			Density	7850 kg/m^3
		Piezoelectric constant d_{31}	-2.1 E + 2 pm/V				
		Capacitance	125 nF				

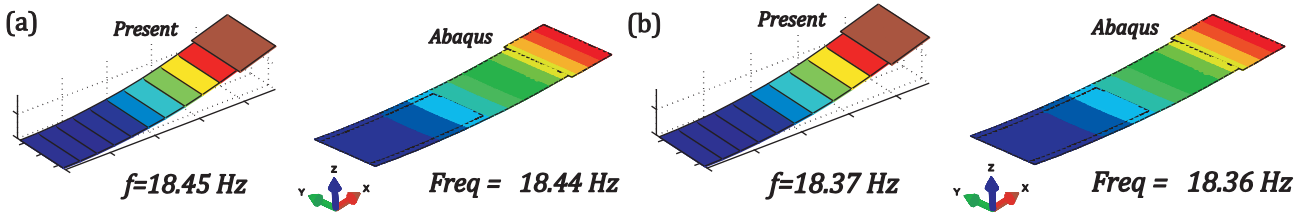

Fig. 5. Natural frequencies at rotation speeds: (a) 1 Hz and (b) 2 Hz.

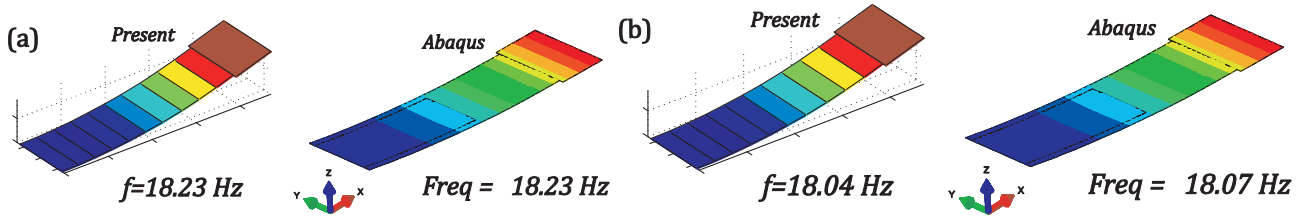

Fig. 6. Natural frequencies at rotation speeds: (a) 3 Hz and (b) 4 Hz.

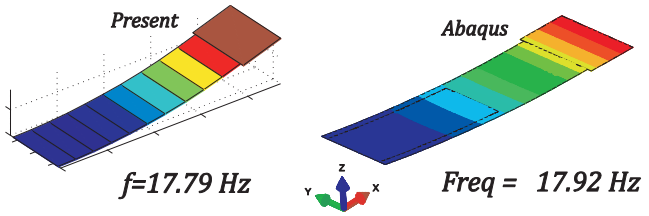

Fig. 7. Natural frequencies at rotation speed: 5 Hz.

6 Hz. The device is mounted on the hub in a similar way to the previous prototype. In all cases a load resistor of 10 kΩ was used due to a limitation in the acquired 5 V voltage of (Arduino-based acquisition system).

The aluminum, steel and spring properties and the material properties specified in the MIDE QP16N supplier data sheet are shown in Table 1.

6. Results

In this section the results of the one-dimensional FE model are compared with numerical simulations and experimental tests. Firstly, the effect of rotation on the natural frequencies is compared with the experimental results and a 3D shell FE model using commercial software (Abaqus). Secondly, the voltage time response, the voltage generation and the power generation are compared with the experimental results considering several rotation speeds.

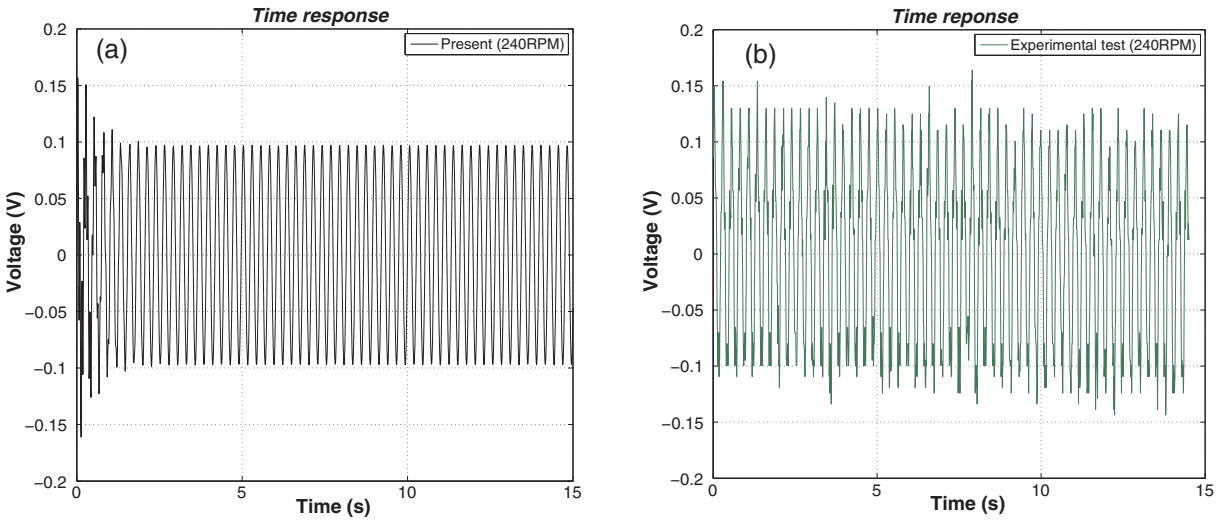

Fig. 8. Voltage time response at 4 Hz: (a) Present formulation, (b) Experimental.

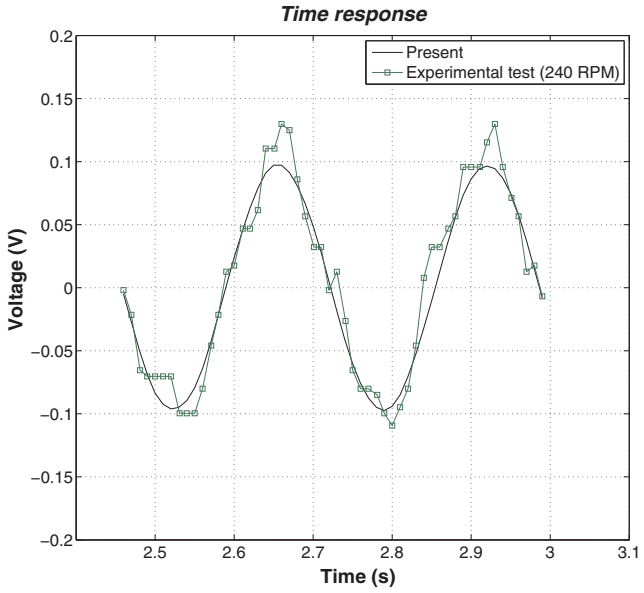

Fig. 9. Voltage time response for the FE model and experimental test at 4 Hz.

6.1. Cantilever beam with a tip mass

6.1.1. Natural frequency validations

The first flexural mode for the non-rotating system is 18.50 Hz for our FE model, 18.40 Hz for the experimental test and 18.47 Hz for the Abaqus simulation. Figs. 5–7 show the normalized modal shapes and frequency values for different rotation speeds comparing the results of our FE model with the Abaqus 3D shell model. In the case of rotation, the spin-softening effect is analyzed for different speeds from 1 Hz to 5 Hz (equivalent to 60–300 rpm). Thus, when this effect is activated due to the centrifugal load, the natural frequencies of the rotating system decrease with increasing rotation speed [1].

It can be observed that our FE model shows a good match with the experimental results and the Abaqus simulation.

6.1.2. Time response

The generalized equations of motion are solved in time using Newmark's time integration method [37] to compare the voltage generation and the time response between the results of our FE model and those of the experimental tests. Fig. 8 shows the voltage time response at a rotation speed of 4 Hz (240 rpm) for 15 s approximately. As presented in this figure, the maximum voltage remains 0.1 V over the interval.

A comparison between our FE model and the experimental results for the voltage time response at 4 Hz (240 rpm) for 0.5 s approximately is presented in Fig. 9. As expected, the time waveform response obtained with the present numerical model is smoother in comparison with the experimental results. This difference may be due to noise fluctuations in the wireless acquisition process.

In energy harvesting, the voltage and power generation parameters are usually analyzed to design an optimum energy harvester. Fig. 10 shows a comparison between the results of our FE model and the experimental test for voltage and power generation for a rotation speed variation from 1 Hz to 5 Hz.

The maximum voltage versus rotating frequency occurs at 5 Hz reaching 0.15 V, respectively. The maximum power obtained occurs at the same rotating frequency (5 Hz) reaching 2.2 μW. This prototype is a typical configuration of an energy harvester, and its analytical solution can be easily found in the literature [21–24]. The aim of this example is to calibrate the electromechanical parameters and study the performance of our model before we evaluate a complex model. It can be observed that the generation of energy increases with rotation speed, and it will continue increasing until the resonance condition is satisfied (see Fig. 7).

6.2. Two beams with a tip mass linked with a spring

6.2.1. Natural frequency validations

When a more complex geometry is required, it is not possible to formulate an analytical solution [26]. For that reason, our proposed FE formulation is useful for modeling complex piezoelectric devices. The first flexural mode for the non-rotating system is 14.07 Hz for our FE model, 14.06 Hz for the experimental test and 14.10 Hz for the Abaqus simulation. The normalized modal shapes and frequency values for rotation speeds from 1 Hz to 6 Hz (60–360 rpm) are shown in Figs. 11–13. In order to obtain convergent results, the FE model built with Abaqus is discretized using S4R shell elements with 4-nodes, reduced integration to avoid shear and membrane locking and hourglass control. The element type SPRING is associated with displacements degrees of freedom, these variables are the force and relative displacement. The mesh contains 659 shell elements and 1 spring element, and the total CPU time to calculate the rotating natural frequencies is

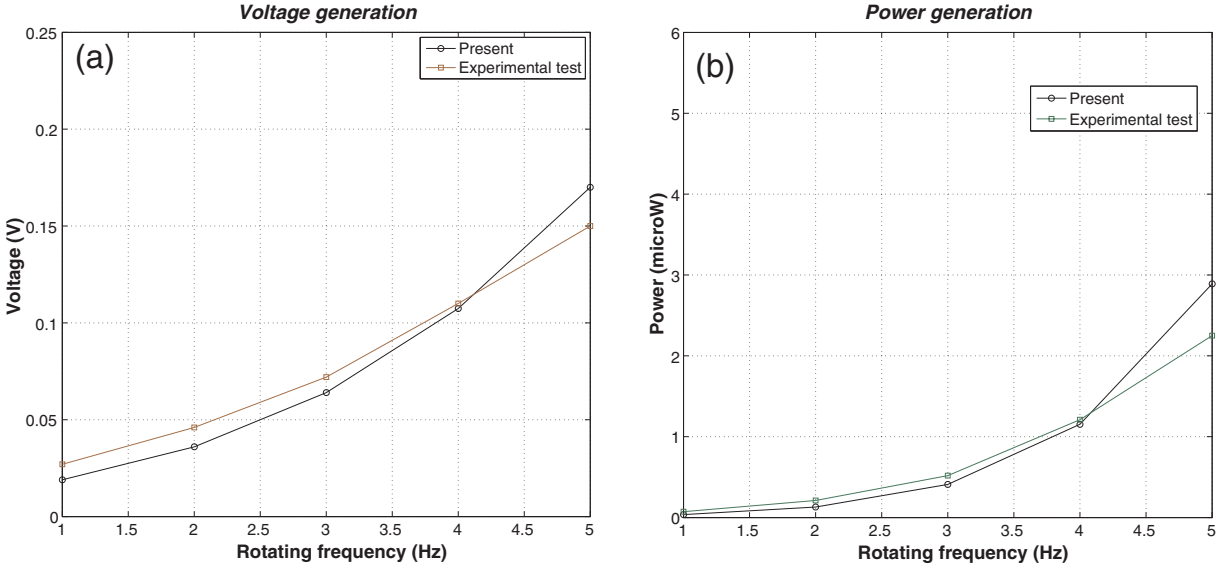

Fig. 10. (a) Voltage generation and (b) Power generation for a rotation speed variation from 1 Hz to 5 Hz.

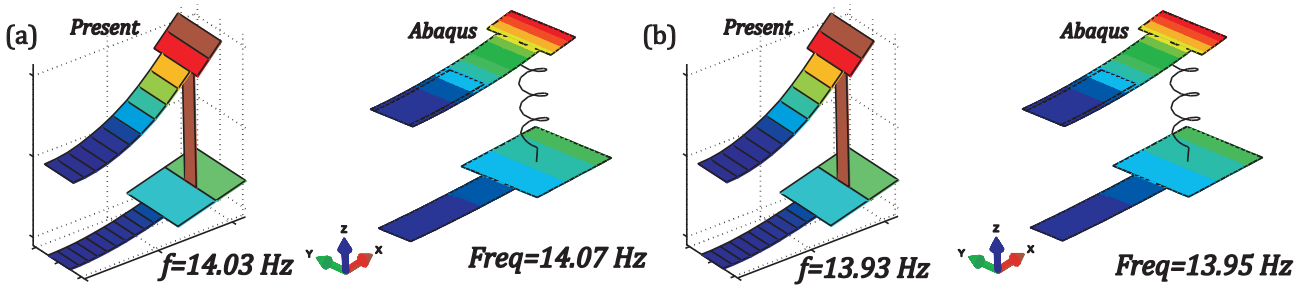

Fig. 11. Natural frequencies at rotation speeds: (a) 1 Hz and (b) 2 Hz.

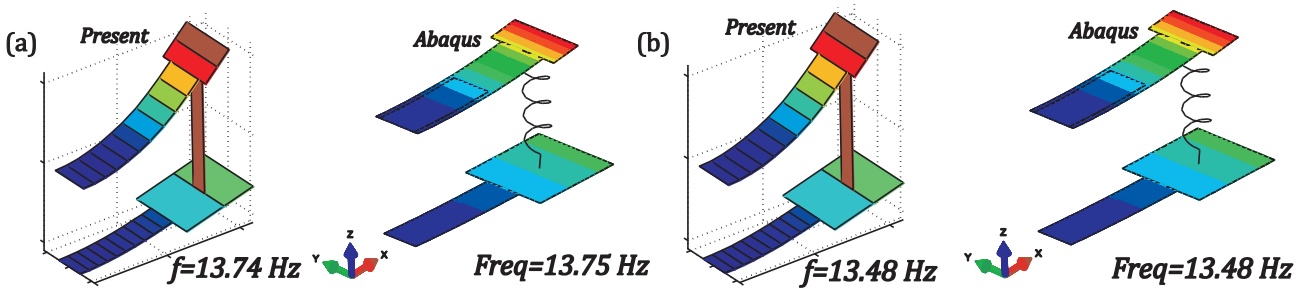

Fig. 12. Natural frequencies at rotation speeds: (a) 3 Hz and (b) 4 Hz.

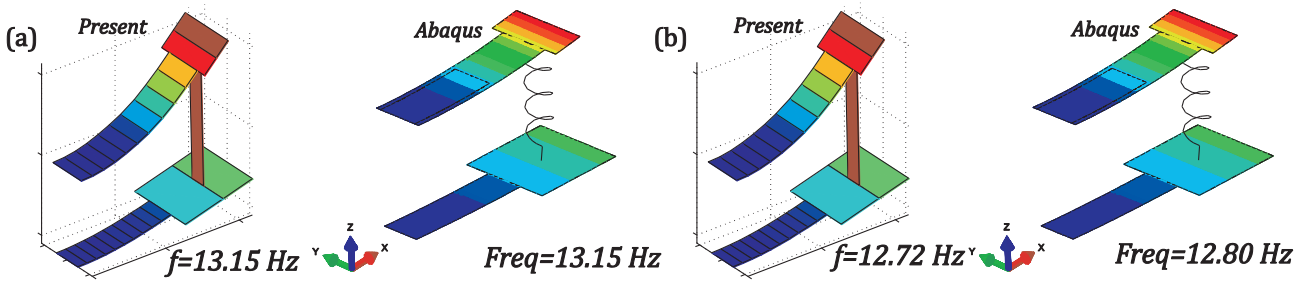

Fig. 13. Natural frequencies at rotation speeds: (a) 5 Hz and (b) 6 Hz.

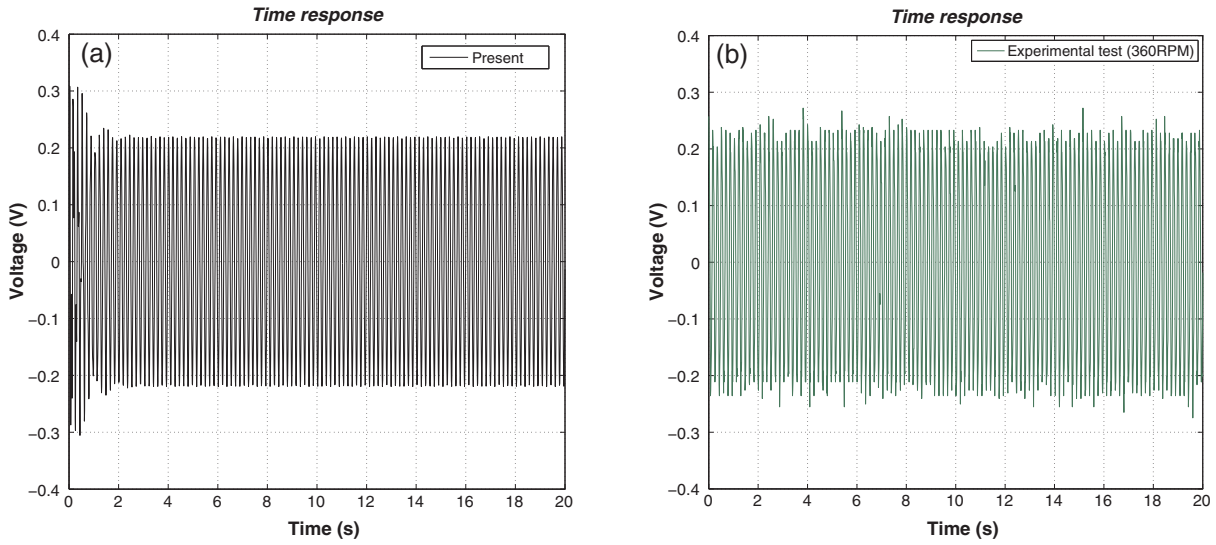

Fig. 14. Voltage time response at 6 Hz (a) Present formulation, (b) Experimental.

80 s. The analysis ∗STATIC is used in Abaqus as the first step of the calculation, together with the option NLGEOM to consider the non-linear geometric effect in the pre-loaded state. Then, in a second step, the procedure ∗Frequency is used for the dynamic analysis of the structure. On the other hand, our FE model is discretized using 24 beam elements and 1 spring element, and the total CPU time is significantly reduced compared to Abaqus, yielding in our case only 0.12 s.

As expected, the natural frequency for the rotating systems decreases with increasing rotation speed. Our FE model shows good agreement with the experimental results and Abaqus simulation. It

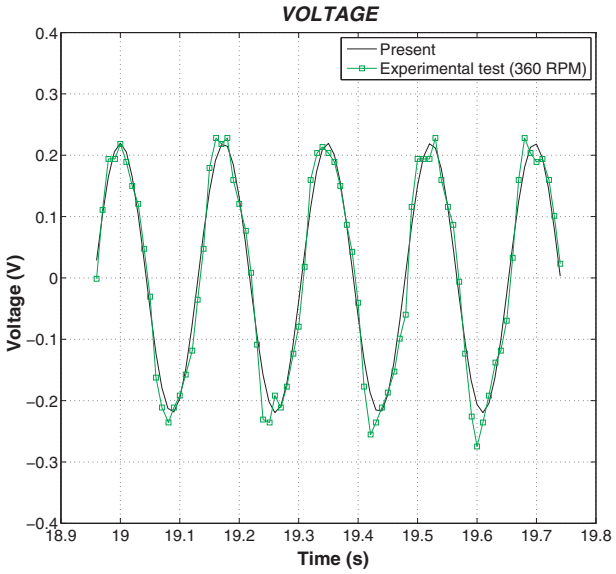

Fig. 15. Voltage time response for the FE model and the experimental test at 6 Hz.

should be noted that the frequency decrease is more pronounced in this case than in the single-beam device.

6.2.2. Time response

Fig. 14 shows the voltage time response at a rotation speed of 6 Hz (360 rpm) for 20 s approximately. The maximum voltage remains 0.21 V over the interval. The prediction of the generated voltage of our FE model is very good compared with the experimental results. As for the computational cost, the elapsed CPU time to solve the time response is 1.73 s.

Fig. 15 presents the voltage time response at 6 Hz (360 rpm) for 1 s approximately (from 18.9 to 19.8 s) for our FE model and the experimental test, which gave a maximum voltage of 0.21 V approximately. It can also be observed that the numerical result gave a similar time waveform response compared with the experimental one.

The peak values of voltage and power output versus the rotation speed from 1 Hz to 6 Hz (60–360 rpm) are presented in Fig. 16.

The results obtained with this FE prototype and the cantilever beam are similar, with the electric generation increasing with rotation speed. The figures above show that the results obtained for our FE model have a good correlation from 1 Hz to 6 Hz rotation speed with respect to the experimental results. The maximum voltage and power generation versus rotating frequency occurs at 6 Hz reaching 0.225 V and 5.5 μW, respectively.

7. Conclusions

The main contribution of this paper is providing a one-dimensional finite element capable of modeling three-dimensional rotational energy harvesting devices. A geometrically nonlinear finite element with linear interpolation was formulated. The finite element was formulated with six mechanical degrees of freedom and one electrical degree of freedom per node. The element matrices were obtained from the Timoshenko beam theory assuming a linear displacement field and a nonlinear strain field in the mechanical domain. As for the electrical domain, a first order theory was formulated. D'Alembert principle was used to derive the electromechanical equilibrium equations of motion. In order to validate our FE formulation, we built two energy harvesting devices to be tested with the aim of getting insights into the generation of electrical power, natural frequencies and time responses. The first prototype to be tested was a cantilever beam with a mass at the free end. This prototype was used to calibrate the electromechanical parameters and analyze the performance of our model. Then a geometrically complex prototype was tested. It consisted of two beams with a mass at the free end linked by a spring. Regarding the experimental tests, an Arduino board with Bluetooth communication protocol (at 115,200 baud) was used to read out the voltage signal from the piezoelectric element in real-time, since Bluetooth receivers are available in almost every mobile device and wireless communication prevents cable connections which may interfere with the testing system. These signals were acquired through the analog input ports on the Arduino board, and subsequently converted using the internal analog-to-digital converter. An application programming interface was developed to establish the Bluetooth connection. A starting/stopping routine of 100 samples per second was set to save the acquired data. The rotating and non-rotating natural frequencies of our FE model were compared with Abaqus simulations and the experimental results. The voltage time signals and power generations of our FE model were compared with the experimental results. The results of our FE model show good accuracy with respect to the experimental results and Abaqus simulations. This work develops, analyzes and verifies a one-dimensional finite element

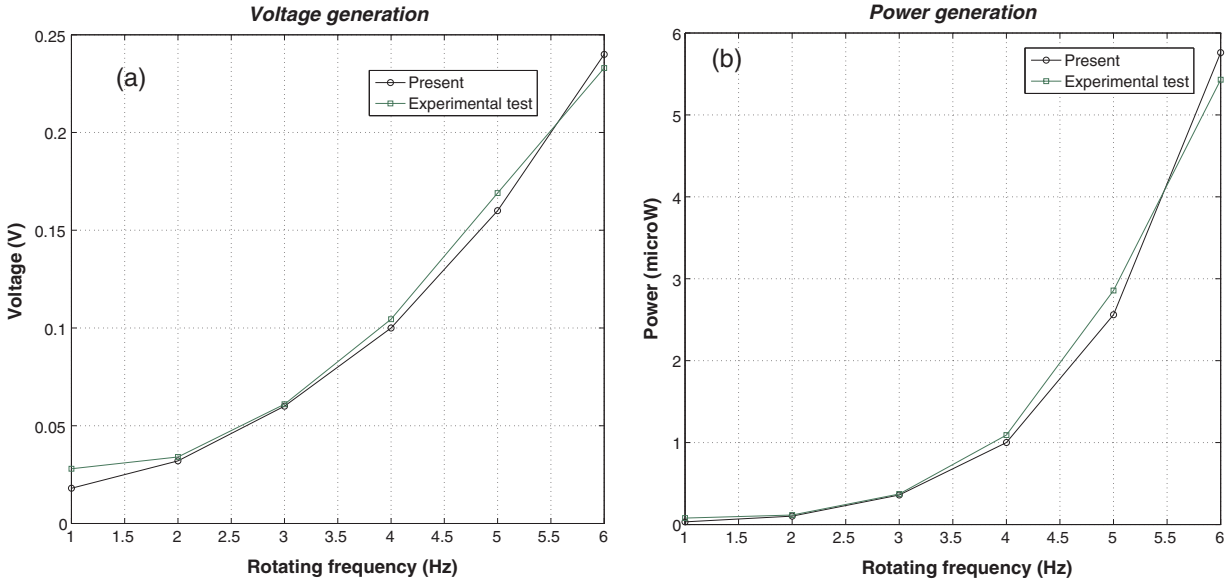

Fig. 16. (a) Voltage generation and (b) Power generation for a rotation speed variation from 1 Hz to 6 Hz.

capable of predicting the dynamical behavior of three-dimensional rotational energy harvesters. In future works, our goal is to develop a more complex rotational energy harvester to investigate the power generation.

Acknowledgements

The authors would like to thank the supports financial from CONICET (PIP N°: 11220120100346), Universidad Nacional del Sur, Universidad Tecnológica Nacional and ANPCyT under grant PICT 2013-2065.

References

[1] Carnegie W. Vibration of rotating cantilever blading: theoretical approaches to the frequency problem based on energy methods. J Mech Eng Sci 1959;1:235–40.
[2] Boyce E, Handelman G. Vibration of rotating beams with tip mass. Appl Math Phys 1961;12:369–92.
[3] Hoa S. Vibration of a rotating beam with tip mass. J Sound Vib 1979;3:369–81.
[4] Geradin M, Kill N. A new approach to finite element modeling of flexible rotors. Eng Comput 1984;1:52–64.
[5] Saravia M, Machado S, Cortínez V. Free vibration and dynamic stability of rotating thin-walled composite beams. Eur J Mech A/Solids 2011;30:432–41.
[6] Choi S, Han M. Vibration control of a rotating cantilevered beam using piezo-actuators: experimental work. J Sound Vib 2003;277:436–42.
[7] Choi S, Park J, Kim J. Vibration control of pre-twisted rotating composite thin-walled beams with piezoelectric fiber composites. J Sound Vib 2006;300:176–96.
[8] Brockmann T, Lammering R. Beam finite elements for rotating piezoelectric fiber composite structures. J Intell Mater Syst Struct 2006;17:431–48.
[9] Beeby SP, Tudor MJ, White NM. Energy harvesting vibration sources for micro-systems applications. Meas Sci Technol 2006;17:R175–95.
[10] Erturk A, Inman DJ. Piezoelectric energy harvesting. Chichester: John Wiley and Sons, Ltd.; 2011.
[11] Erturk A, Inman DJ. A distributed parameter electromechanical model for cantilevered piezoelectric energy harvesters. J Vib Acoust 2008;130. 041002-1.
[12] Erturk A, Inman DJ. An experimentally validated bimorph cantilever model for piezoelectric energy harvesting from base excitations. Smart Mater Struct 2009;18:025009.
[13] Mitcheson PD, Rao GK, Green TC. Energy harvesting from human and machine motion for wireless electronic devices. Proc IEEE 2008;96:1457–86.
[14] De Marqui Junior C, Erturk A, Inman DJ. An electromechanical finite element model for piezoelectric energy harvester plates. J Sound Vib 2009;327:9–25.
[15] Detwiler DT, Shen M, Venkayya VB. Finite element analysis of laminated composite structures containing distributed piezoelectric actuators and sensors. Finite Elem Anal Des 1995;20:87–100.
[16] Kumar A, Sharma A, Kumar R, Vaish R, Chauhan V. Finite element analysis of vibration energy harvesting using lead-free piezoelectric materials: a comparative study. J Asian Ceram Soc 2014;2. 183-143.
[17] Staworko M, Uhl T. Modeling and simulation of piezoelectric elements-comparison of available methods and tools. Mechanics 2008;27:4.
[18] Elvin N, Elvin A. A coupled finite element–circuit simulation model for analyzing piezoelectric energy generators. J Intell Mater Syst Struct 2009;20:587–95.
[19] Zhou L, Sun J, Zheng X, Deng S, Zhao J, Peng S, et al. A model for the energy harvesting performance of shear mode piezoelectric cantilever. Sens Actuat A: Phys 2012;179:85–192.
[20] Lei G, Livernore C. Passive self-tuning energy harvester for extracting energy from rotational motion. Appl Phys Lett 2010;97:081904.
[21] Khameneifar F, Arzanpour S, Moallem M. A piezoelectric energy harvester for rotary motion applications: design and experiments. IEEE/ASME Trans Mechatron 2012;18:1527–34.
[22] Khameneifar F, Moallem M, Arzanpour F. Modeling and analysis of a piezoelectric energy scavenger for rotary motion applications. J Vib Acoust 2010;133. 011005-1.
[23] Guan M, Liao W. Design and analysis of a piezoelectric energy harvester for rotational motion system. Energy Convers Manage 2016;111:239–44.
[24] Shahruz SM, Sundararajan V. Design of energy scavengers mounted on rotating shafts; 2008. Also available at: arXiv:0809.2766.
[25] Yang Y, Shen Q, Jin J, Wang Y, Qian W, Yuan D. Rotational piezoelectric wind energy harvesting using impact-induced resonance. Appl Phys Lett 2014;105:053901.
[26] Hsu Jin-Chen, Tseng Chi-Ta, Chen Yi-Sheng. Analysis and experiment of self-frequency tuning piezoelectric energy harvesters for rotational motion. Smart Mater Struct 2014;23:075013.
[27] Oñate E. Structural analysis with the finite element method: Linear static. Springer; 2013.
[28] Librescu L. Thin-walled composite beams. Springer; 2006.
[29] Reddy JN. An introduction to the finite element method. Mc Graw Hill; 2006.
[30] Tiersten HF. Linear piezoelectric plate vibrations. Springer; 1969.
[31] Butz A, Klinkel S. An anisotropic finite 3D beam element for the analysis of piezoelectric structures. Proc Appl Math Mech 2003;3:262–3.
[32] Barbero E. Finite element analysis of composite materials. Taylor and Francis; 2008.
[33] Meirovitch L. Principles and techniques of vibrations. Prentice Hall; 1997.
[34] Washizu K. Variational methods in elasticity and plasticity. Pergamon Press; 1968.
[35] Zienkiewicz OC, Taylor RL. The finite element method. Butterworth-Heinemann; 2000.
[36] Bilgen O, Erturk A, Inman DJ. Analytical and experimental characterization of macro fiber composite actuated thin clamped-free unimorph benders. J Vib Acoust 2010;132. 051005-1.
[37] Bathe JK. Finite element procedures. Prentice Hall; 1996.